

Disorders of the Nervous System

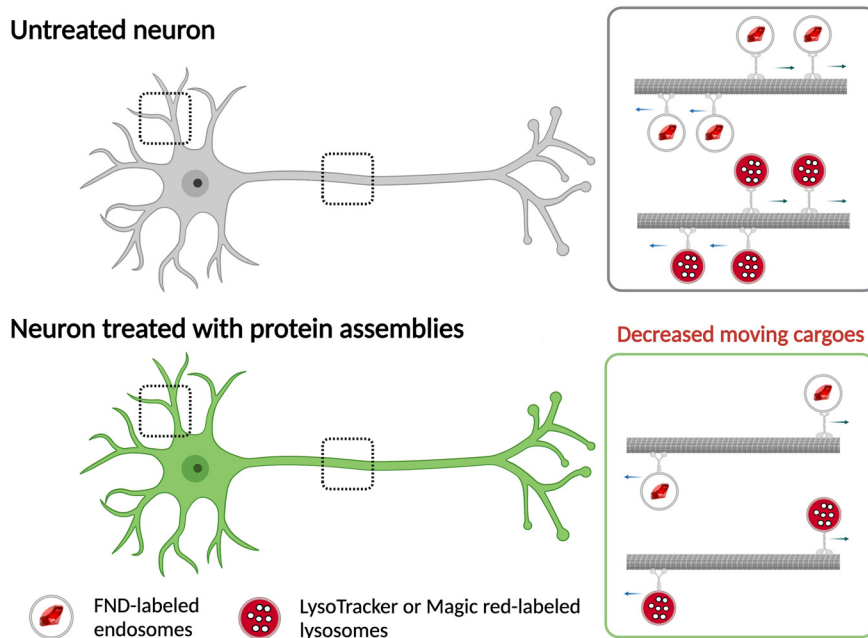
Impact of α -Synuclein Fibrillar Strains and β -Amyloid Assemblies on Mouse Cortical Neurons Endo-Lysosomal Logistics

Qiao-Ling Chou,¹ Ania Alik,² François Marquier,¹ Ronald Melki,² François Treussart,^{1,*} and Michel Simonneau^{1,3,*}

<https://doi.org/10.1523/ENEURO.0227-21.2022>

¹Université Paris-Saclay, École Normale Supérieure Paris-Saclay, Centre National de la Recherche Scientifique, CentraleSupélec, LuMIn, Gif-sur-Yvette 91190, France, ²Laboratory of Neurodegenerative Diseases, Institut François Jacob (MIRGen), Centre National de la Recherche Scientifique, Commissariat à l'Énergie Atomique et aux Énergies Alternatives, Université Paris-Saclay, Fontenay-aux-Roses Cedex 92265, France, and ³Département d'Enseignement et de Recherche en Biologie, École Normale Supérieure Paris-Saclay, Gif-sur-Yvette 91190, France

Visual Abstract



Endosomal transport and positioning cooperate in the establishment of neuronal compartment architecture, dynamics, and function, contributing to neuronal intracellular logistics. Furthermore, dysfunction of endo-lysosomal has been identified as a common mechanism in neurodegenerative diseases. Here, we analyzed endo-lysosomal transport when α -synuclein (α -syn) fibrillar polymorphs, β -amyloid ($A\beta$) fibrils, and oligomers were externally applied on primary cultures of mouse cortical neurons. To measure this transport, we used a simple readout based on the spontaneous endocytosis in cultured neurons of fluorescent nanodiamonds (FNDs), a perfectly stable nano-emitter, and the subsequent automatic extraction and quantification of their directed motions at high-throughput. α -Syn fibrillar polymorphs, $A\beta$ fibrils, and oligomers induce a 2-fold decrease of the fraction of nanodiamonds transported along microtubules, while only slightly reducing their interaction with cortical neurons. This important decrease in moving endosomes is expected to have a huge impact on

Significance Statement

Neurodegenerative diseases are characterized by the deposition of protein aggregates. These proteins exert a broad range of neuronal toxicity. Defects in endo-lysosomal traffic are increasingly viewed as key pathologic features of neurodegenerative diseases, likely contributing to synaptic dysfunction and ultimately neuronal death. Here, we measured by fast fluorescence video-microscopy the endosomal and lysosomal dynamics in the branches of primary culture of mouse cortical neurons after externally applying α -synuclein (α -syn) fibrillar polymorphs (fibrils or ribbons) and β -amyloid ($A\beta$) assemblies (oligomers or fibrils). We provide significant insight into the differential effects of these pathogenic protein assemblies on endosomal and lysosomal transport, and also reveal distinct transport characteristics of the compartments loaded with these protein assemblies compared with endosome ones.

neuronal homeostasis. We next assessed lysosomes dynamics, using LysoTracker. Neurons exposure to $A\beta$ oligomers led to an increase in the number of lysosomes, a decrease in the fraction of moving lysosome and an increase in their size, reminiscent of that found in APP transgenic model of Alzheimer's disease. We then analyzed the effect of α -syn fibrillar polymorphs, $A\beta$ fibrils, and oligomers on endosomal and lysosomal transport and quantified directed transport of those assemblies within cortical neurons. We report different impacts on endosomal and lysosomal transport parameters and differences in the trajectory lengths of cargoes loaded with pathogenic protein assemblies. Our results suggest that intraneuronal pathogenic protein aggregates internalization and transport may represent a target for novel neuroprotective therapeutic strategies.

Key words: α -synuclein; β -amyloid assemblies; endosome; intraneuronal transport; lysosome; mouse cortical neuron

Introduction

Impairment of axonal transport has recently emerged as a factor shared by several neurodegenerative disorders (Morfini et al., 2009; Millicamps and Julien, 2013). Early impact on intraneuronal transport has been thus proposed as a phenotypic trait common to neurodegenerative diseases such as Alzheimer's, Huntington's, and Parkinson's diseases (Stokin et al., 2005; Volpicelli-Daley et al., 2014; Saudou and Humbert, 2016). There is compelling evidence that abnormal protein accumulation in the brain is a key pathophysiological mechanism underlying the neurotoxicity observed in these age-related disorders (Golde et al., 2013; Soto and Pritzkow,

2018). Selective aggregation of misfolded proteins is a hallmark of these neurodegenerative diseases (Saez-Atienzar and Masliah, 2020). An important level of complexity comes from the fact that different species of the same molecules, such as oligomers and fibrils, contribute to a whole spectrum of toxicities (Alam et al., 2019).

Few studies have compared, within the same neurons, fibrillary and oligomeric α -synuclein (α -syn) and β -amyloid ($A\beta$) traffic, which is known to be involved in Parkinson's and Alzheimer's diseases, respectively. Brahic et al., 2016; demonstrated for instance that α -syn, $A\beta_{42}$, and HTTExon1 fibrils are transported anterogradely and retrogradely with different efficiencies in axons of mouse primary neurons grown in microfluidic chambers. Here, we thoroughly quantified the impact of two α -syn fibrillar polymorphs namely fibrils (α -synF) and ribbons (α -synR), $A\beta_{42}$ fibrils ($A\beta F$) and oligomers ($A\beta O$) on endosomal and lysosomal transports in primary cultures of mouse neurons. To measure this transport and investigate finely its parameters, we relied on our previously established method (Haziza et al., 2017), in which we let perfectly stable and nontoxic fluorescent nanodiamonds (FNDs) being spontaneously internalized by neurons in endosomes, then follow their displacement by fast video-microscopy and finally apply to the videos our analysis pipeline to extract and analyze single particle trajectories automatically. Using fluorescently-labeled α -syn and $A\beta$ assemblies, we conducted the same investigations on their own intraneuronal transport.

Our data allow to address three complementary questions: (1) do α -synF, α -synR, $A\beta F$, and $A\beta O$ influence the fraction of cargoes moving along the microtubules; (2) do they impact the dynamics of intracellular endosomal and lysosomal transport?

Received May 20, 2021; accepted January 25, 2022; First published April 25, 2022.

The authors declare no competing financial interests.

Author contributions: F.T. and M.S. designed research; Q.-L.C. performed research; A.A., F.M., and R.M. contributed unpublished reagents/analytic tools; Q.-L.C. analyzed data; F.T. and M.S. wrote the paper.

*F.T. and M.S. contributed equally to this work.

This work was supported by the Joint Program on Neurodegenerative Disease Research and Agence National de la Recherche Contract TransPathND ANR-17-JPCD-0002 (to M.S. and R.M.), Euronanomed III contract MoDiaNo ANR-18-ENM3-0002 (to M.S.) and the Fondation pour la Recherche Médicale Contract ALZ201912009776 (to R.M.). Q.-L.C. was supported by a PhD scholarship from Taiwan Ministry for Education, University Paris-Saclay and JPND TransPathND (ANR-17-JPCD-0002), and Euronanomed III contract MoDiaNo (ANR-18-ENM3-0002).

Correspondence should be addressed to François Treussart at francois.treussart@ens-paris-saclay.fr or Michel Simonneau at michel.simonneau926@gmail.com.

<https://doi.org/10.1523/ENEURO.0227-21.2022>

Copyright © 2022 Chou et al.

This is an open-access article distributed under the terms of the Creative Commons Attribution 4.0 International license, which permits unrestricted use, distribution and reproduction in any medium provided that the original work is properly attributed.

We show here that all pathogenic protein assemblies reduce the fraction of endosomes moving along microtubules and impact some of their transport parameters. Furthermore, lysosomes properties (number, fraction of lysosomes moving and transport parameters) are also affected by $A\beta O$. Finally, our data indicate that cargoes loaded with α -synF, α -synR, $A\beta F$, or $A\beta O$ are transported differently from endosomes, considered as control cargoes, which suggests distinct molecular characteristics of cargo-motor assemblies.

Materials and Methods

Production of α -syn fibrillar assemblies, $A\beta$ fibrils, and oligomers

The expression and purification of human wild-type (WT) α -syn was performed as previously described (Ghee et al., 2005). Pure WT α -syn was incubated in buffer A to obtain the fibrillar polymorph “fibrils” α -synF (50 mM Tris-HCl at pH 7.5, 150 mM KCl) and in buffer B for “ribbons” α -synR (5 mM Tris-HCl at pH 7.5) at 37°C under continuous shaking in an Eppendorf Thermomixer set at 600 rotations per minute (rpm) for 4–7 d (Bousset et al., 2013). The fibrillar α -syn polymorphs were centrifuged twice at $15,000 \times g$ for 10 min and resuspended twice in PBS at 3 g/l (or 215 μ M) before labeling with ATTO 488 NHS-ester (#AD 488–3, Atto-Tec) fluorophore following the manufacturer’s instructions using a protein:dye ratio of 1:2. The labeling reactions were arrested by addition of 1 mM Tris (pH 7.5). The unreacted fluorophore was removed by a final cycle of two centrifugations at $15,000 \times g$ for 10 min and resuspensions of the pellets in PBS. This labeling protocol typically yields ≥ 1 ATTO molecule incorporated per α -syn monomer on average as previously demonstrated (Shrivastava et al., 2015). The assemblies were examined by transmission electron microscopy after adsorption on 200 mesh carbon-coated electron microscopy grids and negative stained with 1% uranyl acetate before and after fragmentation using a JEOL 1400 electron microscope (JEOL).

The expression and purification of Met- $A\beta$ 1–42 was performed as described (Walsh et al., 2009). $A\beta$ was assembled in PBS, at 4°C or 37°C without shaking for 2 or 24 h to obtain oligomers $A\beta O$ or fibrils $A\beta F$, respectively. The two kinds of assemblies were labeled with ATTO 488 NHS-ester at a protein:dye ratio of 1:2. The labeling reactions were arrested by addition of 1 mM Tris at pH 7.5. For fibrillar $A\beta$, the unreacted fluorophore was removed by two cycles of centrifugation and resuspension of the pelleted fibrils in PBS as described for α -syn. For oligomeric $A\beta$, the oligomers were separated from the monomeric and fibrillar forms of the protein by size exclusion chromatography on a Superose 6 HR10/300 column (GE Healthcare, Life Sciences) equilibrated in PBS pH 7.4 at a flow rate of 0.5 ml/min. Elution was monitored by measuring absorbance at 280-nm wavelength. The Superose 6 column was calibrated with Dextran blue (over 2200 kDa), thyroglobulin (670 kDa), β -amylase (200 kDa), BSA (66 kDa), and carbonic anhydrase (29 kDa) standards (Sigma-Aldrich).

Primary mouse cortical neuron cultures

We used commercial primary mouse cortical neurons (ref. Invitrogen A15586, ThermoFisher) because the provider quality check guarantees a purity of 98% of neurons. The cells were grown on high optical quality glass coverslips (high-precision $170 \pm 5 \mu$ m thick, 18-mm diameter, ref. 0117580, Marienfeld GmbH). The coverslips are first cleaned with 70% ethanol, rinsed with water for injection (ref. A128730, ThermoFisher) and exposed during 1 h to UV light. They were then coated with 0.1 mg/ml poly-L-ornithine (ref. P3655, Sigma-Aldrich Merck KGaA) and placed for 2 h in an incubator set at 37°C, then rinsed twice with water and let dry at biological hood for 1 h. We plated an amount of 6×10^5 primary mouse cortical neurons on each coated coverslip, which was then put at the bottom of a 6-wells plate, each well being finally filled with 3 ml of neurobasal phenol red-free medium (ref. 12348017, ThermoFisher) containing 0.5 mM GlutaMax (ref. 35050061, ThermoFisher), 2% B-27 (ref. 17504044, ThermoFisher) and 1% PenStrep (ref. 15070063, ThermoFisher). The 6-well plate was then placed in an incubator at 37°C and 5% CO_2 . Half of the volume of the medium was replaced with fresh medium 24 h after plating. We made the subsequent medium changes every 3 d to reduce glutamate toxicity. Neurons were grown until 21 d in culture (DIC).

Exposure of mouse cortical neurons to α -syn fibrillar assemblies, $A\beta$ fibrils, or oligomers

In all the measurements dealing with (1) the impact of pathogenic protein assemblies on endosomal-lysosomal transport; (2) their colocalization with FND-labeled compartment or lysosomes; or (3) the tracking of their intraneuronal transport by fluorescence video-microscopy, cortical neurons were incubated with either 0.2 μ M ATTO 488-labeled α -synF or R, or 1 μ M ATTO 488-labeled $A\beta F$ or $A\beta O$.

α -SynF or R were added at 24, 48, or 72 h before observations, while the addition time was either 24 or 48 h for ATTO 488-labeled $A\beta F$ or $A\beta O$. The video acquisitions of all the experiments were performed at 21 DIC.

Washing protocol to test the protein assemblies interaction with the neuron membrane

The coverslips with the culture attached to them were extracted from the well and flushed with PBS first and then twice with culture medium, before FND internalization was conducted, following the procedure described in the next paragraph.

Intraneuronal transport cargo labeling

To evaluate the endosomal transport parameters, we relied on our FND assay (Haziza et al., 2017). We used commercially available sized 35 nm FND (brFND-35, FND Biotech). Each NP contains an average of 15 nitrogen-vacancy emitters displaying a peak emission wavelength around 700 nm and a full-width at half-maximum of ≈ 100 nm. This far-red emission allows also to investigate the colocalization of green-emitting ATTO 488-labeled neurodegenerative-disease related species with FND-labeled cargoes. FND were internalized in cortical neurons

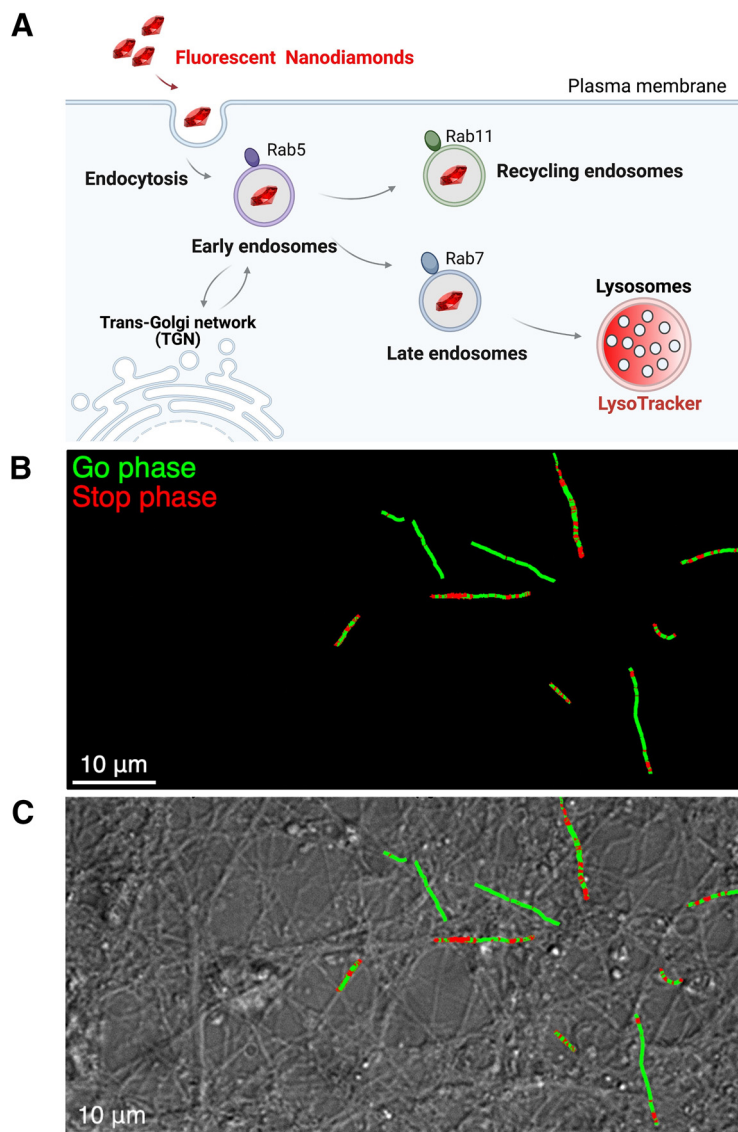


Figure 1. Recording FND trajectories in mouse cortical neurons at DIC21. **A**, Schematic representation of the cargoes that are tracked thanks to FND, at different stages after their endocytosis. We previously showed (Haziza et al., 2017) that FND are present in cargoes at different stage of their lifetime after endocytosis, as shown by colocalization measurements with specific membrane protein markers: Rab5 for early endosome; Rab7 for late endosome; Rab11 for recycling endosome; LysoTracker for the lysosome. **B**, Illustration of FND trajectories with go (green) and stop (red) phases. **C**, Differential interference contrast images of cortical neurons overlapped with 10 representative trajectories. Scale bar: 10 μ m.

just before the transport analysis, at DIC21. Each culture coverslip was removed from the six-well plate containing maintaining medium and put in contact with 400 μ l of fresh culture medium to which we added 2 μ l of stock solution of FNDs (1 mg/ml), reaching a final FND concentration of 5 μ g/ml. After 10-min incubation, the extra FND-containing medium was absorbed by a wiper sheet and the coverslip was placed back to the dish containing the old maintaining medium. The culture was then placed back during 20 min in the incubator before the video acquisition.

To measure lysosomal transport or investigate the colocalization of neurodegenerative disease-related species with lysosomes, cortical neurons were stained at DIC21, just before the observation, with LysoTracker Deep Red (ref. L12492, ThermoFisher) or Magic Red Cathepsin B

substrate (ref. ICT937, Bio-Rad). These dye molecules have an emission spectrum within the similar range than the one of FND. The coverslip was removed from maintaining medium and incubated with prewarmed (37°C) culture medium containing 50 nM LysoTracker or Magic Red (1:20 dilution) for 1 h. The probe-containing medium was replaced with the old maintaining medium and followed by video acquisition.

Pseudo-total internal reflection (TIRF) live-cell video-microscopy

Pseudo-TIRF illumination was implemented on an inverted microscope (Eclipse Ti-E, Nikon) as described in details in (Haziza et al., 2017). The whole microscope is

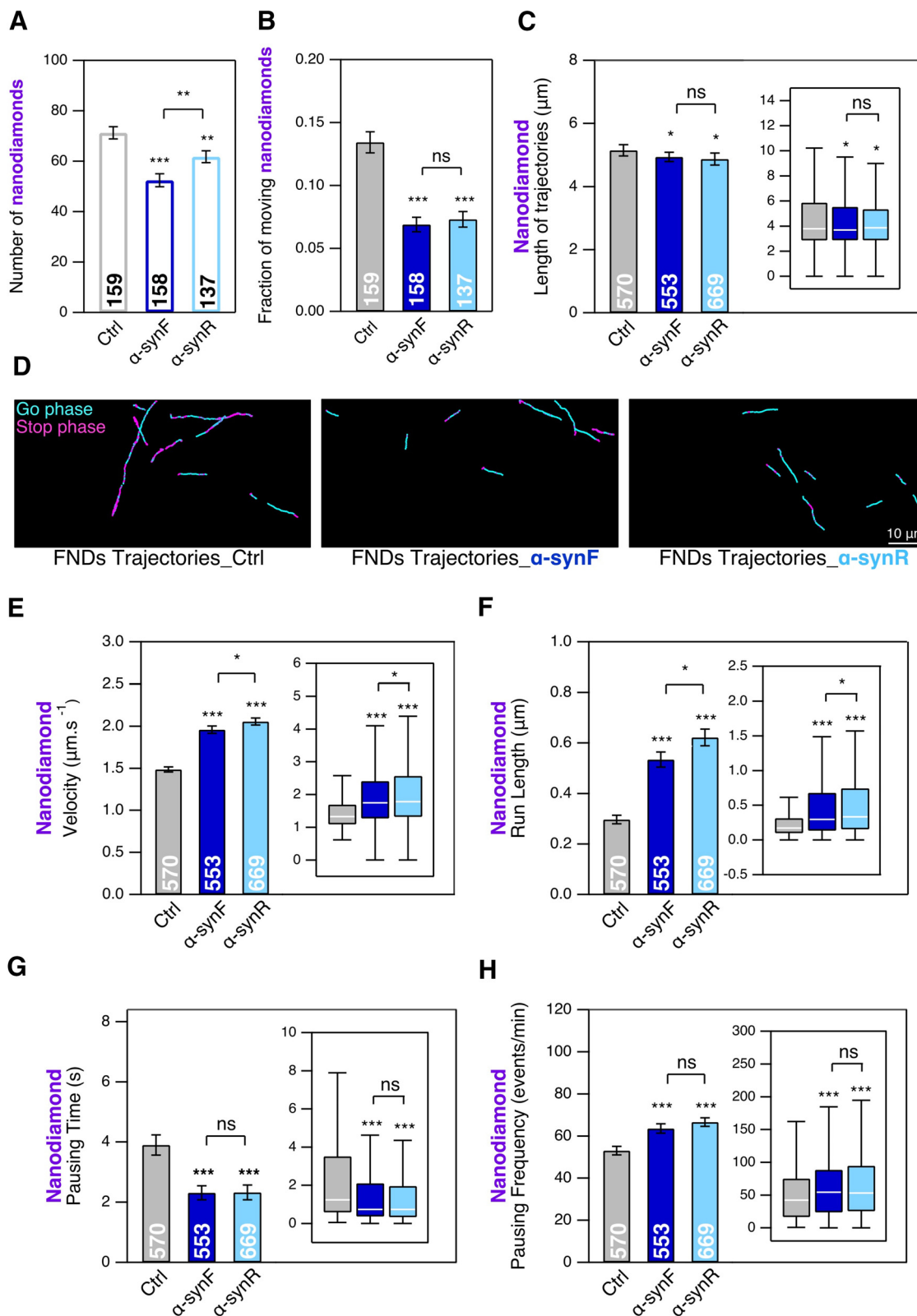


Figure 2. Effect of α -synF or R on the mobility of endosomes and their transport as measured by tracking FND-containing cargoes in mouse cortical neurons at DIC21; 24-h exposure to α -synF or R at 0.2 μ M concentration, compared with nothing added control (Ctrl). **A**, Number of FNDs detected per FoV of 40 \times 80 μ m size during 2 min of observation. **B**, Fraction of FNDs-containing cargoes having a directed motion. **C**, Length of FND trajectories. **D**, Examples of FND trajectories. Scale bar: 10 μ m. **E-H**, Comparison of four transport parameters: (**E**) curvilinear velocity, (**F**) run length, (**G**) pausing time, and (**H**) pausing frequency. The number within each bar represents the total number of FoVs (**A**, **B**) or trajectories (**C**, **E-H**) analyzed from $n = 8$ coverslips (4 independent cultures).

continued

Insets, Box-plots representation of the same dataset. * and *** mean $p < 0.05$ and $p < 0.001$ respectively; ns: non significant. See also Extended Data Figures 2-1, 2-2.

enclosed in a cage incubator (Okolab) to maintain temperature at 37°C. For the intraneuronal transport recording, each coverslip supporting the neuron culture is mounted at the bottom of a Ludin chamber (type 1, Life Imaging Service), installed inside the environmental chamber (in which 5% partial CO₂ pressure and 100% humidity is maintained) having a hole at its bottom allowing direct optical access of the microscope objective to the coverslip. We used a $\times 100$ magnification and 1.49 numerical aperture immersion oil objective (CFI Apo TIRF $\times 100$ Oil, Nikon), compatible with differential interference contrast mode. Field of views (FoVs) of interest of the neuron cultures were selected in white-light illumination differential interference contrast mode. Two continuous-wave lasers are coupled to the microscope and fluorescence was recorded on a cooled EMCCD array detector (DU-885K-CS0, Andor Technologies) of 1004×1002 pixels, with 80-nm pixel size in the sample plane. Two-minute duration videos were acquired at 20 full frame/s rate, large enough to be able to detect short pausing duration in cargoes displacements. EMCCD parameters were selected to provide the largest signal-to-background ratio for FND label tracking at the selected frame rate, leading to EM gain of 90, preamplification gain $3.8\times$, and digitalization speed of 35 MHz. FNDs and LysoTracker fluorophore were excited with a diode-pumped solid-state laser at a wavelength of 561 nm (SLIM-561-100, Oxixus S.A.), while ATTO 488 dye was excited with a laser diode emitting at a wavelength of 488 nm (LBX-488-200-CSB-PP, Oxixus S.A.). Each excitation laser power was adjusted so that the detection dynamic range of all channels was identical for the above mentioned fixed EMCCD settings. This leads to 561-nm laser excitation power of 60 mW for FND, 200 μ W for LysoTracker and 1 mW for Magic Red, and to 488-nm laser excitation power of 200 μ W for ATTO 488 dye.

To perform two-color acquisitions and record simultaneously FND (or LysoTracker) and ATTO 488 we combined the two laser beams with a dual-band dichroic filter (ref. Di01-R488/561, Semrock), and placed a dual imaging system (W-VIEW GEMINI, Hamamatsu) in front of the EMCCD array detector. This system splits half of the detection FoV in two color channels with a dichroic beamsplitter (FF560-FDi01, Semrock) and projects each color on half of the array detector, further preceded by bandpass detection filters (red channel: HC697/75, Semrock; green channel: ET525/50, Chroma Corporation). The result is that each frame of the video contains the same rectangular FoV (1004×501 pixels) in green (ATTO 488) and red (FND and LysoTracker) emission range, allowing to identify spots that colocalize dynamically.

Video processing and intraneuronal transport quantification

Two programs written in python were developed to extract quantitative parameters from videos automatically.

The first one relies on Trackpy 0.4.2 package (Allan et al., 2019), from which it uses two functions: “locate” to identify isolated spots in each fluorescence frame and fit them with gaussians, and “link” which connects the spots between frames to form trajectories using Crocker–Grier algorithm (Crocker and Grier, 1996). Transport parameters are then calculated with a second program which first parses each trajectory into “go” and “stop” phases based on the confinement ratio calculation as described in (Haziza et al., 2017), with a threshold set to 0.8 for this parameter, the “go” phase phases corresponding to confinement ratio larger to this value. Four main transport parameters are extracted for each trajectory: velocity, which is the average speed of all go phases; run length: average distance traveled during all go phases; pausing time: average duration of the stop phases, and pausing frequency (events/min). In addition to these four main parameters, we also calculated the total length of the trajectory as the sum of all run lengths during go phases.

Lysosomes size estimation

To get an estimate of the lysosome size from the diffraction limited fluorescence images, we considered the LysoTracker spots as the result of the convolution of the microscope point spread function (assimilated to a Gaussian of standard deviation, SD, σ_{PSF}) and the lysosome assimilated to a symmetrical Gaussian of SD σ_L . The result of this convolution is also a Gaussian of SD σ_T , related to σ_L and σ_{PSF} by $\sigma_T^2 = \sigma_{\text{PSF}}^2 + \sigma_L^2$. σ_T is the so-called “size” output of the Trackpy locate function. The knowledge of σ_T and σ_{PSF} allows the derivation of σ_L . We then defined the lysosome “diameter” d_L as the full width at half maximum of its Gaussian approximation, inferred by $d_L = 2\sqrt{2\ln 2}\sigma_L$. For the PSF size σ_{PSF} we took the measured value of the smallest FND spot observed in several trajectories with our microscope. This value was $\sigma_{\text{PSF}} = 112$ nm, consistent with the theoretical Airy radius $\rho_A = 286$ nm (diffraction limit at 700-nm maximum emission wavelength for the 1.49 numerical aperture objective used), and the empirical relation $\sigma_{\text{PSF}} = \frac{\rho_A}{3}$, giving here an experimental PSF SD of $286/3 = 95$ nm.

Quantification of fluorescence intensity of ATTO 488-labeled α -synF in cortical neuron branches

We quantify the fluorescence intensity from the first frame of the green channel videos, using Fiji ImageJ software (Schindelin et al., 2012). We first identify from the differential interference contrast image some well-separated and mainly straight neuronal branches, that we surround with the region-of-interest (ROI) polygonal selection tool as close as possible to the branch to include all the fluorescence signal, over a length of 30 μ m. We then used the

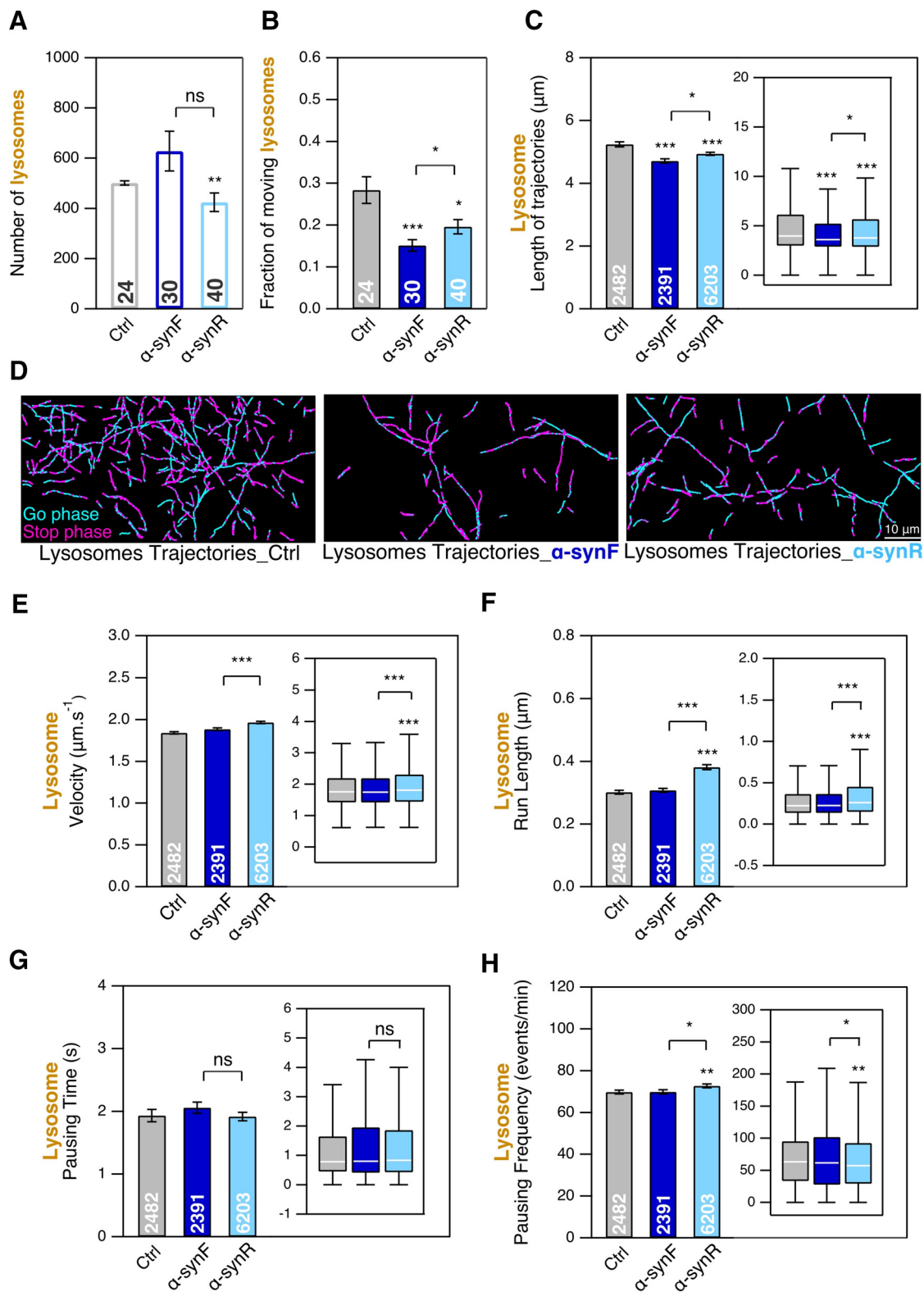


Figure 3. Effect of α -synF or α -synR on the mobility of LysoTracker-labeled lysosomes and their transport in mouse cortical neurons at DIC21; 24-h exposure to α -synF or α -synR at 0.2 μ M concentration, compared with nothing added control (Ctrl). **A**, Number of lysosomes detected per FoV of 40 \times 80 μ m size during 2 min of observation. **B**, Fraction of lysosomes having a directed motion. **C**, Length of lysosome trajectories. **D**, Examples of lysosome trajectories. Scale bar: 10 μ m. **E-H**, Comparison of four transport parameters: curvilinear velocity (**E**), run length (**F**), pausing time (**G**), and pausing frequency (**H**). The number within each bar represents the total number of FoVs (**A**, **B**) or trajectories (**C**, **E-H**) analyzed from $n=2$ coverslips (from one culture). Insets, Box-plots representation of the same dataset. *, ** and *** mean $p < 0.05$, $p < 0.01$ and $p < 0.001$ respectively; ns: non significant.

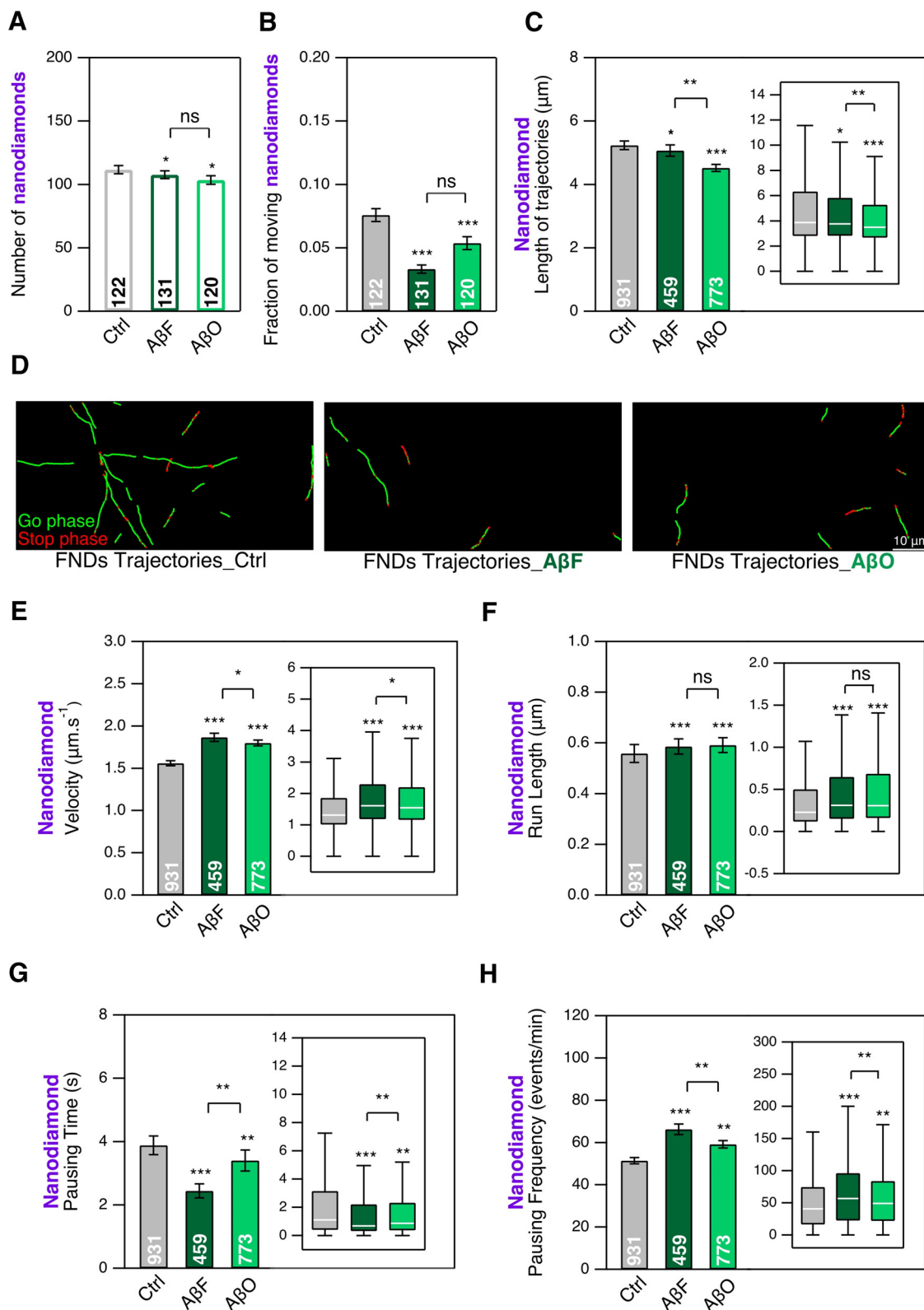


Figure 4. Effect of AβF and AβO on the mobility of endosomes and their transport as measured by tracking FND-containing cargoes in mouse cortical neurons at DIC21; 24-h exposure to AβF and AβO at 1 μm concentration, compared with nothing added control (Ctrl). **A**, Number of FNDs detected per FoV of 40 × 80 μm size during 2 min of observation. **B**, Fraction of FNDs-containing cargoes having a directed motion. **C**, Length of FND trajectories. **D**, Examples of FND trajectories. Scale bar: 10 μm. **E-H**, Comparison of four transport parameters: curvilinear velocity (**E**), run length (**F**), pausing time (**G**), and pausing frequency (**H**). The number inside the bar represents the total number of FoVs (**A**, **B**) or trajectories (**C**, **E-H**) analyzed from *n*=6 coverslips (3

continued

independent cultures). Insets, Box-plots representation of the same dataset. *, ** and *** mean $p < 0.05$, $p < 0.01$ and $p < 0.001$ respectively; ns: non significant. See also Extended Data Figure 4-1.

Analyze function to measure the average intensity counts per pixel in the defined ROI, to which we subtract the average background counts, measured after having moved the ROI in a region without branches.

Data representation and statistical analysis

All bar plots display the \pm SEM of the distribution. Box plots display the median value as the horizontal line within the box whose limits are 25% and 75% percentiles; bottom and top horizontal lines correspond to 10th and 90th percentiles. As all the data compared between two conditions were random and normally distributed but with unequal variance (as tested with a *F* test), we performed the relevant comparison test which is the nonparametric Wilcoxon Mann–Whitney two-tailed (implemented in Igor Pro 8, Wavemetrics Inc.). Stars referred to the following *p*-value significance level: * $p < 0.05$, ** $p < 0.01$, *** $p < 0.001$.

Results

Quantification of intraneuronal transport using FNDs

We quantified the intraneuronal transport with our FND tracking assay (Haziza et al., 2017). We first used a simple readout consisting in counting the number of FND detected in FoVs of size $40 \times 80 \mu\text{m}$ during 2 min. We selected each FoV based on the criteria that it contains approximately the same density of neuronal branches, as estimated from differential interference contrast images (Fig. 1). Our incubation protocol was designed to strongly limit any nonspecific interactions of FND, like their attachment to the coverslip supporting the culture, and favor their interaction with neuron membranes and their subsequent internalization in endosomes (Haziza et al., 2017). The perfectly stable fluorescence of FND allows to reconstruct the endosome trajectories accurately and identify “go” and “stop” (none or very slow motion) phases (Fig. 1B) in the transport of FND-labeled endosomes along neuronal branches as observed in differential interference contrast microscopy (Fig. 1C).

α -SynF and R affect the number of cargoes transported along microtubules without major changes in trajectory length

Primary cultures of mouse cortical neurons were incubated at DIC20 with α -synF or R at a concentration of $0.2 \mu\text{M}$ for 24 h. The intraneuronal transport in these cultures was investigated at DIC21.

Both exposures to α -synF or R led to a small decrease (26% for α -synF and 13% for α -synR) in the number of FND (moving or not) present in each FoV, indicating that both fibrillar polymorphs impact the FND binding to neuronal membrane and their transport dynamics within neurons (Fig. 2A). Indeed, if we consider the fraction of these FND having a directed motion, corresponding to

those being first internalized in endosomes and then taken in charge by molecular motors, we observed that it decreases by 49%, on exposure of neurons to α -synF and 45% in the case of α -synR (Fig. 2B). The unknown mechanism involved in such a large decrease in the number of cargoes transported along microtubules is expected to impair the functions of cortical neurons.

In order to determine whether this important reduction of FND moving fraction is related to the binding of the protein assemblies to the neuronal membrane, possibly leading to a reduced endocytosis, we tried in the case of α -synF to wash away the aggregates just before the addition of FND (Materials and Methods), but we found that the interaction of the nanodiamonds with neuron did not change in washed-neuron condition compared with unwashed (Extended Data Fig. 2-1A–C); in particular, we did not observe differences in the fraction of moving FND. We concomitantly measured the amount of ATTO 488-labeled assemblies along the neuronal branches (as quantified by the dye fluorescence intensity) and could not see any differences before and after washing (Extended Data Fig. 2-1D,E), which is in agreement with FND–neuron interaction results, and indicate a strong binding of α -synF to the neuronal membrane.

Using our established FND-based intraneuronal transport assay (Haziza et al., 2017) we detected and quantitatively analyzed the alternation of movement and pause phases of intraneuronal cargoes motion. We first measured the length of trajectories (see Materials and Methods) for control FND and FND in the presence of either α -synF or α -synR. We did not evidence any major differences between these conditions (Fig. 2C,D; decrease of 4% for α -synF and 5% for α -synR).

We then measured four parameters: the curvilinear velocity of each moving phase, its run length, the duration of the pauses and the pausing frequency. The velocity (Fig. 2E) and run length (Fig. 2F) increases (velocity: 31% and 38%; run length: 80% and 100%, for α -synF and R, respectively), the pausing time decreases (Fig. 2G; 40% decrease for both fibrillar assemblies), while the pausing frequency increases (Fig. 2H; 19% and 25%, for α -synF and R, respectively). These results are summarized in Extended Data Figure 2-2A.

We next analyzed the same parameters for lysosomes labeled with LysoTracker red, an established marker of lysosomes, with the difference, compared with FND, that all the fluorescent spots, including the static ones, correspond to lysosomes because LysoTracker only become fluorescent once inside lysosomes. α -synR treatment induces a slight but significant decrease (15%) in the number of lysosomes per FoV, while α -synF does not (Fig. 3A). This result suggests that α -synR reduce the endocytosis. It is consistent with the observed decrease of FND interacting with neuron (Fig. 2A) that possibly reveals their reduced uptake. Furthermore, like for endosomes (Fig. 2B), α -synF and R induce a 46% and 32% decrease,

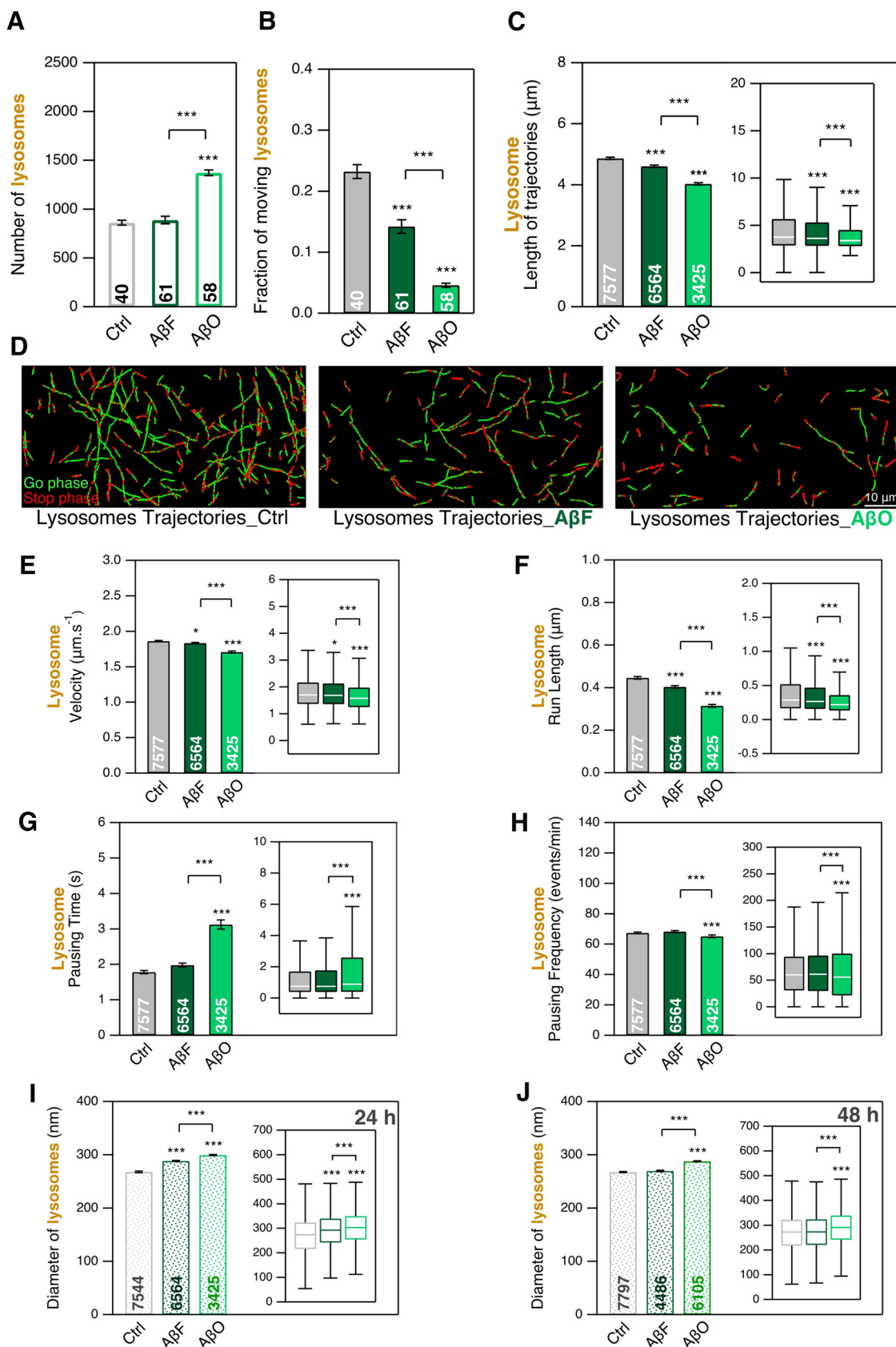


Figure 5. Effect of AβF and AβO on the mobility of LysoTracker-labeled lysosomes and their transport in mouse cortical neurons at DIC21; 24-h exposure to AβF and AβO at 1 μM concentration, compared with nothing added control. **A**, Number of lysosomes

continued

detected per FoV of $40 \times 80 \mu\text{m}$ size during 2 min of observation. **B**, Fraction of lysosomes having a directed motion. **C**, Length of lysosome trajectories. **D**, Examples of lysosome trajectories. Scale bar: $10 \mu\text{m}$. **E–H**, Comparison of four transport parameters: curvilinear velocity (**E**), run length (**F**), pausing time (**G**), and pausing frequency (**H**). **I, J**, Comparison of lysosome size. The number inside the bar represents the total number of FoVs (**A, B**), trajectories (**E–H**), and lysosomes (**I, J**) analyzed from $n=2$ coverslips (from one culture). Insets, Box-plots representation of the same dataset. * and *** mean $p<0.05$ and $p<0.001$ respectively. See also Extended Data Figures 5-1, 5-2, 5-3.

respectively, in the fraction of lysosomes having a directed motion (Fig. 3B). Analysis of lysosome trajectory lengths indicates a slight decrease (Fig. 3C; 9% and 3% for α -synF and R, respectively). Example of FoV showing lysosome trajectories in the different conditions are shown in Figure 3D, where the large decrease in the fraction of lysosomes having a directed motion can be clearly seen.

We quantified the same transport parameters for lysosomes than for FND, using the same experimental paradigm. In contrast to what we observed for endosomes transport, exposure of neurons to α -synF did not lead to any changes in lysosomes transport parameters (Fig. 3E–H). Interestingly, however, in cortical neurons exposed to α -synR, we measured a slight increase of 6% in lysosomes velocity (Fig. 3E) and larger one of 26% in run length (Fig. 3F), no significant change in pausing time (Fig. 3G), and a slight increase of 4% in pausing frequency (Fig. 3H). These results are summarized in Extended Data Figure 2-2B.

A β assemblies affect the number of cargoes transported along microtubules without major changes in trajectory length

We also analyzed the same parameters after mouse cortical neurons exposure to either A β F or A β O at DIC20, for 24 h, followed by intracellular transport measurement at DIC21. We used the common $1 \mu\text{M}$ concentration that has been reported to have a biological impact (Marshall et al., 2020). Figure 4A shows a slight decrease (3% and 7% for A β F and A β O, respectively) of FND interacting with neurons exposed to A β F or A β O, accompanied by a much larger decrease (56% and 29% for A β F and A β O, respectively) of the fraction having directed motions (Fig. 4B). FND trajectory lengths stay almost the same for A β F (3% decrease) but are reduced by A β O (Fig. 4C,D; 13% decrease). We also investigated the effect of A β assemblies at the smaller concentration of $0.2 \mu\text{M}$, identical to the one of α -syn assemblies. Even at this lower concentration, we could detect for both A β F and A β O small decreases (19% and 18% for A β F and A β O, respectively) in the number of FND per FoV (Extended Data Fig. 4-1A) and in the fraction of FND having a directed motion (Extended Data Fig. 4-1B; 11% and 18% for A β F and A β O, respectively). To summarize, as for α -syn assemblies (Fig. 3), the exposure of cortical neurons to A β assemblies induce important and significant decreases of the endosomal transport.

We then measured more precisely the impact of A β F and A β O on endosomal transports parameters. We observed an increase of FND velocity (Fig. 4E; 20% and

15% for A β F and A β O, respectively) and run length (Fig. 4F; 5% and 7% for A β F and A β O, respectively), a decrease in their pausing time (Fig. 4G; 36% and 12% for A β F and A β O, respectively) and an increase of the pausing frequency (Fig. 4H; 28% and 15% for A β F and A β O, respectively), with effects more pronounced for A β F than for A β O. Interestingly, the same trends of changes were also observed at the lower A β F and A β O concentration of $0.2 \mu\text{M}$ (Extended Data Fig. 4-1C–F). Let us finally point out that for A β F, the important changes of some transport parameters overall combine in an only very slight decrease in trajectory length as shown in Figure 4C, which makes the detailed quantitative analysis performed all the more useful. These results are summarized in Extended Data Figure 2-2A.

Regarding the impact of A β on lysosomal transport, we noticed large differences between the two types of assemblies A β F and A β O. In neurons exposed to A β O, the total number of lysosomes detected in a FoV as compared with controls increased by 50% (Fig. 5A) while it stayed unchanged in case of exposure to A β F. The intracellular transport measurements we performed showed that the fraction of moving lysosomes decreased by 1.6-fold and 5.7-fold in neurons exposed to A β F and A β O, respectively (Fig. 5B; from 23% for control to 14% for A β F and 4.5% for A β O). Lysosome trajectory lengths were only slightly decreased for A β F (5%) and more significantly reduced for A β O (Fig. 5C,D; 17% decrease) exposure.

We also measured lysosome transport parameters in the presence of $1 \mu\text{M}$ A β F or A β O (Fig. 5E–H). For A β F, we observed almost no change in velocity (Fig. 5E), pausing time (Fig. 5G), and pausing frequency (Fig. 5H). In contrast, exposure to A β O, led to a 1.7-fold increase of the pausing time. The run length decreased significantly for both assemblies (Fig. 5F; with 9% and 13% decrease for A β F and A β O exposure, respectively). These results are summarized in Extended Data Figure 2-2B.

Furthermore, as changes in lysosome size was described in APP mouse transgenic model of Alzheimer's disease (Gowrishankar et al., 2015), we asked whether detectable changes in lysosome diameter can be quantified on 24- or 48-h exposure to $1 \mu\text{M}$ A β F and A β O. We detected a slight increase (7%) of lysosome diameter on exposure of neurons to A β F at 24 h that disappears at 48 h. This contrasts with the increase we observed at both time points (11% and 7% at 24 and 48 h, respectively) in neurons exposed to $1 \mu\text{M}$ A β O (Fig. 5I,J; Extended Data Fig. 5-1A–C). The finding that A β O addition triggers an increase in lysosomes number and size and a decrease in lysosome movements is in agreement with previous reports (Gowrishankar et al., 2015; Marshall et al., 2020).

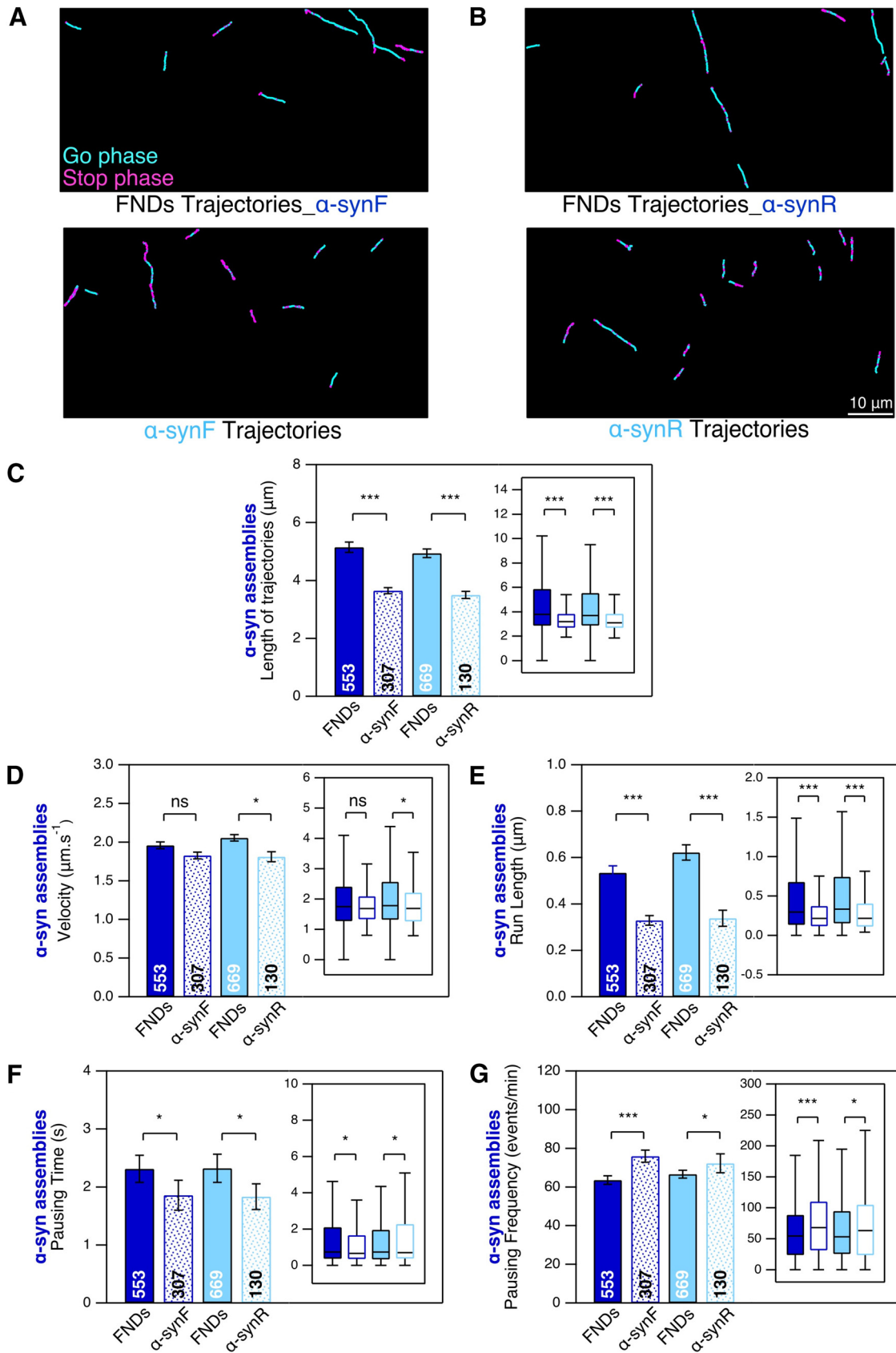


Figure 6. Intraneuronal transport of ATTO 488-labeled α-synF and R in mouse cortical neurons at DIC21. DIC20 cortical neurons were exposed to α-synF and R during 24 h, at concentration of 0.2 μM. **A, B**, Examples of α-synF and R, and FND trajectories (in

continued

the presence of α -synF and R). Scale bar: 10 μ m. **C**, Length of α -synF, α -synR, and FND trajectories. **D–G**, Comparison of four transport parameters: curvilinear velocity (**D**), run length (**E**), pausing time (**F**), and pausing frequency (**G**). The number inside the bar represents the total number of trajectories analyzed from $n = 8$ coverslips (4 independent cultures) is indicated in each bar. Insets, Box-plots representation of the same dataset. * and *** mean $p < 0.05$ and $p < 0.001$ respectively; ns: non significant.

Finally, as LysoTracker can also label acidic compartments other than lysosomes, in particular late endosomes, we repeated the transport experiment with Magic Red substrate that reveals by fluorescence the Cathepsin B protease activity, taking place more specifically in lysosomes. We observed that for both α -synF (Extended Data Fig. 5-2) and $A\beta$ F (Extended Data Fig. 5-3) Magic Red-labeled compartments (lysosomes) behaved the same as LysoTracker-labeled ones for all parameters, with in particular a $\approx 40\%$ decrease of the mobile fraction of Magic Red and LysoTracker-labeled compartment in the presence of the fibrillar assemblies. These results indicates that, in our case, LysoTracker and Magic Red labeling largely overlap and that we can rely on LysoTracker puncta density to quantify endocytic activity as we did. These results are summarized in Extended Data Figure 2-2C.

Transport of α -syn and $A\beta$ assemblies within cortical neurons

We also assessed α -syn and $A\beta$ assemblies transport within cortical neurons while documenting their impact on endosomes and lysosomes dynamics. As ATTO 488 dye used to label α -syn and $A\beta$ assemblies exhibit no emission spectrum overlap with neither FND nor LysoTracker deep red, we were able to measure simultaneously the transport properties of endosome or lysosome and the assemblies on two-color channels.

We first studied α -syn fibrillar assemblies transport (Fig. 6). We found that α -synF and R display directed movements as shown by examples of trajectories in Figure 6A,B. We compared these motions to the endosomal transport in the presence of α -syn fibrillar polymorphs. Interestingly, α -syn F and R trajectories are $\sim 29\%$ shorter than those of FND (Fig. 6C). We also compared the transport parameters and found smaller velocity (Fig. 6D; 5% and 10% for α -synF and α -synR, respectively), run length (Fig. 6E; 39% and 46% for α -synF and α -synR, respectively), and pausing time (Fig. 6F; 19% and 21% for α -synF and α -synR, respectively) for α -synF and α -synR-loaded cargoes compared with those of FND-containing endosomes. On the contrary, α -synF and R pausing frequencies were larger than those of FND (Fig. 6G; 19% and 8% for α -synF and α -synR, respectively). The shorter trajectories length and run-length together with the larger pausing frequency, suggest that cargoes loaded with α -synF- and R are transported less efficiently than those containing FND.

Similarly, we also investigated ATTO 488-labeled $A\beta$ F and $A\beta$ O intraneuronal transport (Fig. 7) at the concentration of 1 μ M, as we could not detect their fluorescence signal at 0.2 μ M. Both species exhibit directed transport as shown by examples of trajectories in Figure 7A,B. These trajectories are shorter than the ones of FND in the same conditions (Fig. 7C), as for α -syn fibrillar assemblies.

Regarding the transport parameters, compared with FND, $A\beta$ F, and $A\beta$ O have slightly larger velocity (Fig. 7D; 8% and 12% for $A\beta$ F and $A\beta$ O, respectively), and a trend toward a shorter run-length (Fig. 7E; 7% and 28% for $A\beta$ F and $A\beta$ O, respectively). As for α -syn fibrillar assemblies, $A\beta$ F and $A\beta$ O exhibit a much shorter pausing time (Fig. 7F; 49% and 53% for $A\beta$ F and $A\beta$ O, respectively) and a much larger pausing frequency (Fig. 7G; 41% and 36% for $A\beta$ F and $A\beta$ O, respectively). The shorter trajectories length and run-length together with the larger pausing frequency suggest that, like in the case of α -syn, cargoes loaded with $A\beta$ F and $A\beta$ O are transported less efficiently than those containing FND.

Moreover, since differences in $A\beta$ O and $A\beta$ F uptake in cultured neurons were recently reported (Vadukul et al., 2020), we also investigated the related aspect of the number of $A\beta$ assembly trajectories per FoV at 24- and 48-h time points (Extended Data Fig. 7-1). We did not observe differences in the number of trajectories 24 h after addition of the assemblies (Extended Data Fig. 7-1A) in agreement with (Vadukul et al., 2020); see their Figure 4B. However, at 48-h time point, we measured a ≈ 2.5 lower number of $A\beta$ O trajectories compared with $A\beta$ F ones (Extended Data Fig. 7-1B), which differs to uptake results of (Vadukul et al., 2020) at 72-h time point, who reported a ≈ 1.5 times larger amount of internalized $A\beta$ O compared with $A\beta$ F (sonicated). Our observations differ from (Vadukul et al., 2020), but several reasons may explain this discrepancy: (1) we quantify only the moving fraction of $A\beta$ assemblies; (2) we do not have the 72-h point; and finally (3) we do not use the exact same $A\beta$ F.

Finally, we assessed in a quantitative manner the co-localization of α -syn and $A\beta$ assemblies with lysosomes, as a function of neuron exposure time at 24 and 48 h (Fig. 8). While the fraction of α -syn fibrillar assemblies moving within lysosomes increases from $\approx 4\%$ at 24 h to 12–14% at 72 h (Fig. 8A), it reaches already $\approx 41\%$ at 24 h for $A\beta$ fibrils continuing its increase up to $\approx 51\%$ at 48 h (Fig. 8B). $A\beta$ O moving in or with lysosomes have slightly lower colocalization proportions, however much larger than for α -syn fibrillar assemblies. We repeated these analyses with Magic Red labeling instead of LysoTracker for α -synF (Extended Data Fig. 8-1A) and $A\beta$ F (Extended Data Fig. 8-1B) at 24 h and achieved similar results, with a $\approx 40\%$ colocalization fraction of $A\beta$ F with Magic Red-labeled lysosomes, and only $\approx 7\%$ for α -synF.

Discussion

In this work, we investigated the generic effects of α -syn fibrillar polymorphs (fibrils and ribbons) and $A\beta$ assemblies (oligomers and fibrils) on endosomal and lysosomal movements in mouse cortical neurons. In neurons, early endosomes and lysosomes move using different types of machinery. Also, the former are compartmentalized

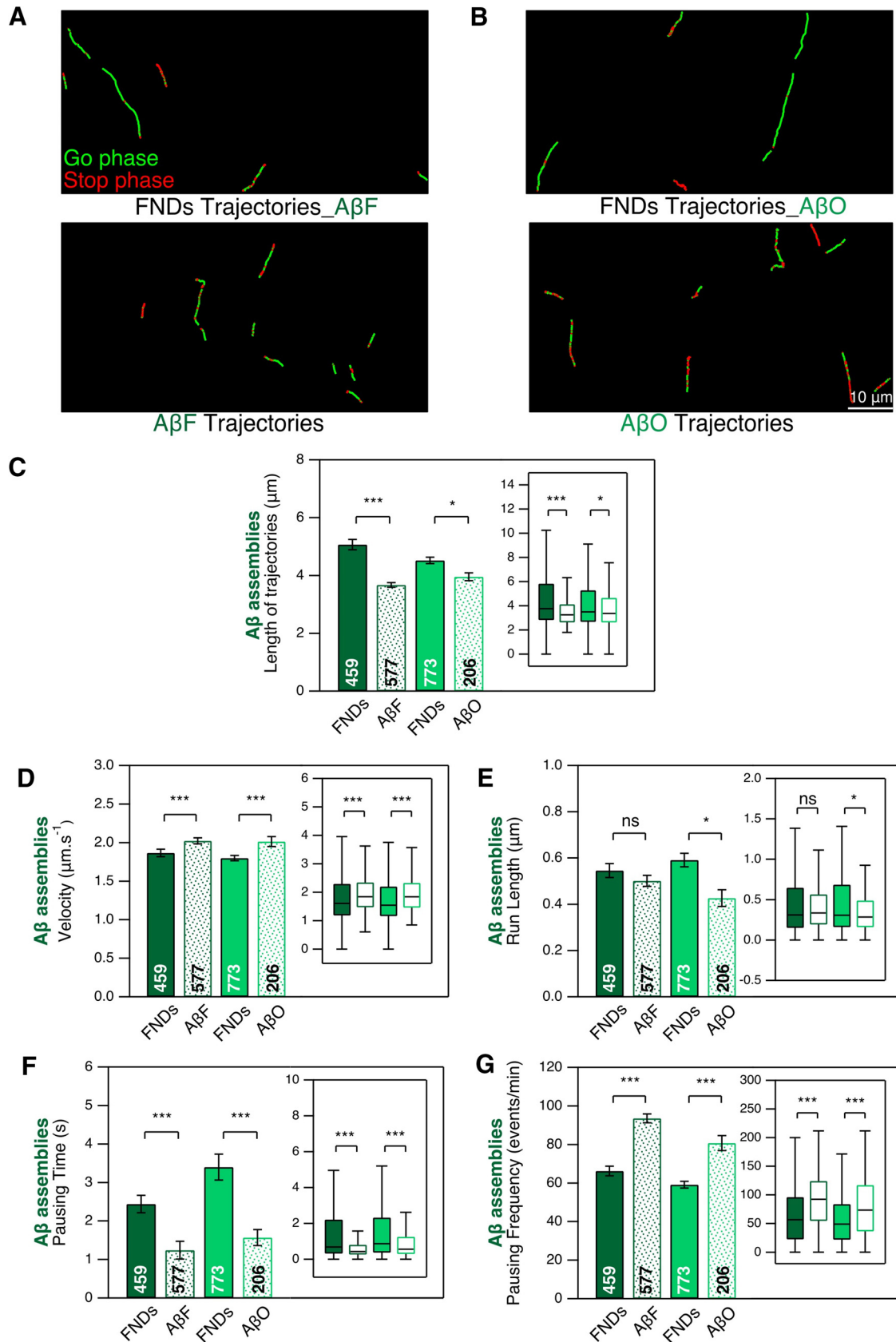


Figure 7. Intraneuronal transport of ATTO 488-labeled AβF and AβO in mouse cortical neurons at DIC21. DIC20 cortical neurons were exposed to AβF and AβO (1 μm) during 24 h. **A, B**, Examples of trajectories. Scale bar: 10 μm. **C**, Length of AβF, AβO and

continued

FND trajectories. **D–G**, Comparison of four transport parameters: curvilinear velocity (**D**), run length (**E**), pausing time (**F**), and pausing frequency (**G**). The number inside the bar represents the total number of trajectories analyzed from $n=6$ coverslips (from 3 independent cultures) is indicated in each bar. Insets: box plots representation of the same dataset. * and *** mean $p<0.05$ and $p<0.001$ respectively; ns: non significant. See also Extended Data Figure 7-1.

(dendrites vs axon) while the latter are not (Winckler et al., 2018). However, because of the high density of the cultures it was not possible to identify unambiguously the compartment (dendrite or axon) in which the traced vesicles moved, and therefore we could not study separately the impact of the protein assemblies on axonal and dendritic endolysosomal transports.

Potential consequences of a decrease in the number of cargoes transported at a given time within cortical neurons

The exposure of cortical neurons to α -syn and $A\beta$ assemblies led to important reductions (between 32% and 56%) of moving endosomes and lysosomes along neuronal branches (Figs. 1, 2). We previously showed that pathogenic α -syn and $A\beta$ assemblies bind the plasma

membrane with, as a consequence, a redistribution of essential membrane proteins (Renner et al., 2010; Shrivastava et al., 2013, 2015). We further reviewed the physico-pathogenic mechanisms at the origin and resulting from pathogenic proteins assemblies-plasma membrane components interactions (Shrivastava et al., 2017). The reduction we report here might result from changes in membrane dynamics and endocytosis rate.

Exposure of cortical neurons to α -syn and $A\beta$ assemblies affected moving FND-containing endosome properties. α -Syn fibrillar assemblies increased their velocity by 31–38% and run length by 80–100% (Fig. 2E,F) and decreased their pausing time by 40% (Fig. 2G) while increasing their pausing frequency to a lesser extend (19–25%; Fig. 2H). We observed similar effects but less pronounced for moving FND-containing endosomes when neurons are exposed to $A\beta$ F or $A\beta$ O (Fig. 4E–H). These changes

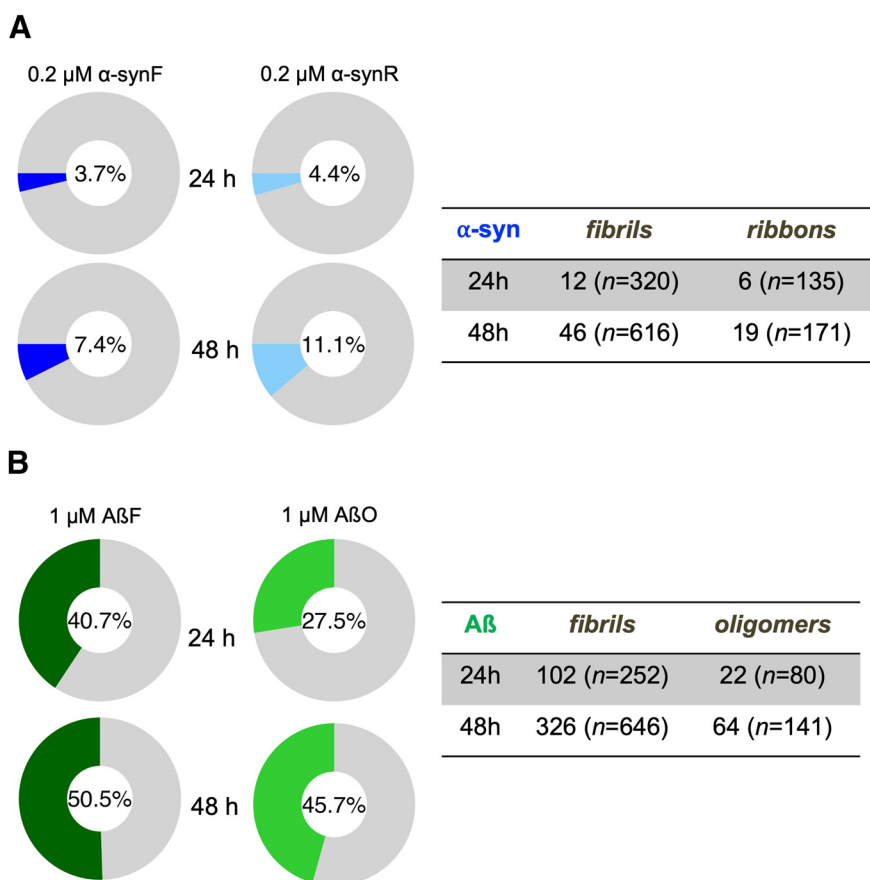


Figure 8. Colocalized events between moving neurodegenerative disease-related molecular species and moving lysosomes at different time points. **A**, α -synF and α -synR were incubated for 24 and 48 h, at concentration of $0.2 \mu\text{M}$. **B**, $A\beta$ F and $A\beta$ O were incubated for 24 and 48 h, at concentration of $1 \mu\text{M}$. The number inside the donut plot represents the percentage of moving α -syn or $A\beta$ assemblies colocalized with lysosomes (LysoTracker labeled). The table on the right panel indicates the number of neurodegenerative-related molecular species trajectories colocalized with lysosomes. n represents the total number of trajectories. The percentage and number of trajectories in each time point were analyzed from two coverslips (from one culture). See also Extended Data Figure 8-1.

reflect an increase in mobility of moving FND-containing endosomes. Hence, while decreasing the fraction of moving FND-labeled endosomes, α -synF and R or A β F and A β O, increase the overall mobility of the moving ones (Extended Data Fig. 2-2A).

A decrease in the number of moving endosomes or lysosomes can affect protein quality control, accompanied by limited elimination of damaged membrane and cytosolic proteins, protein aggregates, and membranous organelles (Winckler et al., 2018). Furthermore, considering that lysosomes and late endosomes act as mRNA translation platforms (Cioni et al., 2019; Liao et al., 2019; Fernandopulle et al., 2021), changes in the number of cargoes transported at a given time within a cortical neuron is expected to dramatically impact mRNA translation platform either in dendrites or in axons. In particular, the regulation of protein synthesis and degradation at the neuronal synapse is local and dynamic and modify the synaptic proteome autonomously during plasticity (Giandomenico et al., 2022). Hence, the synaptic function can be impacted if the number of moving lysosomes is affected.

Effect of α -syn and A β assemblies on lysosomes transport

We observed that α -synF (Fig. 3E–H) and A β F (Fig. 5E–H) barely impact the lysosomal transport parameters as compared with the control. In contrast, α -synR (Fig. 3E–H) and A β O (Fig. 5E–H) induce significant changes of lysosomes transport parameters (Extended Data Fig. 2-2B). Furthermore, the size of lysosomes significantly increased in the presence of A β O (Fig. 5I,J). This set of impairments of lysosomal transport in Alzheimer-related context are in full agreement with previous reports (Gowrishankar et al., 2015; Marshall et al., 2020). Indeed, using a mouse model of Alzheimer's disease (Gowrishankar et al., 2015) evidenced axonal lysosome accumulations with local impairment in the retrograde axonal transport of lysosome precursors. Similarly, Marshall et al. (2020) found that misfolded A β ₄₂ impacts the endo-lysosomal pathway. They reported impairments in the uptake of proteins that use a dynamin-dependent endosomal mechanism and accumulation of lysosomes.

Intraneuronal transport of neurodegenerative-related molecular species

We were able to quantify the intraneuronal transport parameters for α -syn and A β pathogenic species (Figs. 6, 7). We found that cargoes loaded with α -synF and R exhibit a more dynamical transport compared with those containing FND that are characterized by a larger pausing frequency and shorter run-length and pausing time (Fig. 6D–G). A β F and A β O-containing endosomes exhibit similar characteristics (Fig. 7D–G) with in addition an increase in velocity, not observed for α -synF and R. These results suggest that similar molecular mechanisms are at play in the transport of the two α -syn fibrillar polymorphs, the A β F and A β O. However, the \approx 7-fold larger fraction of A β F and A β O found in moving lysosomes compared with α -syn assemblies (Fig. 8), also indicate differences in the molecular interactions of A β assemblies

with lysosomes. These results suggest a cellular triage leading to differential transport of α -syn and A β assemblies.

Potential application in drug discovery assay

We report here the use of a model based on primary mouse cortical neurons where it is possible to identify a robust decrease in the number of vesicles moving intracellularly (Figs. 2B, 3B, 4B, 5B), in the order of 30–50%, and up to 5-fold for lysosomes in neurons exposed to A β O (Fig. 5B). Such a large decrease is likely to impact the physiology of neurons and it is reasonable to consider that the transport of other cargoes, such as mitochondria and RNA granules, is also affected. This endolysosomal transport impairment endophenotype can be instrumental in generating large-scale drug-discovery campaigns (i.e., $>10^5$ compounds) as used in more complex human cellular models (Park et al., 2021).

The cargoes transport blockade within cortical neurons we report could either result from a direct interaction between pathogenic aggregates and the intraneuronal transport machinery or a pathogenic aggregates-mediated transcriptional changes in transport proteins expression (Lee et al., 2004; Encalada and Goldstein, 2014; Guo et al., 2020). Analysis of neuronal immunoprecipitates of α -syn fibrillar assemblies and A β polymorphs may be instrumental to identify the molecular partners that directly interact with these protein assemblies. A recent postmortem proteomics study identified proteins whose abundance changed at different stages of Alzheimer's disease (Li et al., 2021). At its early stage, differentially expressed proteins of “clathrin-coated endocytic vesicle membrane” (GO: 0030669) and the secretory pathway (R-HSA-432720: “Lysosome Vesicle Biogenesis” and R-HSA-432722: “Golgi Associated Vesicle Biogenesis”) classes were over-represented. Comparison of proteome profile changes in our neuronal model with (Li et al., 2021) profiles can be instrumental to identify druggable targets to enhance the number of transported cargoes.

Finally, we quantified intraneuronal transport of neurodegenerative-linked molecular species (α -syn fibrillar polymorphs, A β F, and oligomers) whose transport characteristics are distinct from those of endosomes but for which no molecular characterization is yet available. Furthermore, we observed that all these protein assemblies are transported intracellularly in cortical neurons with very similar quantitative characteristics. We could not detect differences in their transport parameters. Further work will be required to identify a possible common transport mechanism and the specific molecules involved in this transport. This identification can then be harnessed to selectively inhibit this transport.

These results also need to be considered from the standpoint of the prion-like spread of pathogenic protein particles between neurons (Brundin et al., 2010; Hardy and Revesz, 2012; Jucker and Walker, 2018). Selective inhibition may avoid the spread of these neurotoxic species. Thus, advances in the identification of targets involved in cargoes loaded with pathogenic protein aggregates transport may lead to novel neuroprotective therapeutic avenues.

References

- Alam P, Bousset L, Melki R, Otzen DE (2019) α -Synuclein oligomers and fibrils: a spectrum of species, a spectrum of toxicities. *J Neurochem* 150:522–534.
- Allan DB, Caswell T, Keim NC, van der Wel CM (2019) soft-matter/trackpy: Trackpy v0.4.2 (v0.4.2). Zenodo. <https://doi.org/10.5281/zenodo.3492186>.
- Bousset L, Pieri L, Ruiz-Arlandis G, Gath J, Jensen PH, Habenstein B, Madiona K, Olieric V, Böckmann A, Meier BH, Melki R (2013) Structural and functional characterization of two alpha-synuclein strains. *Nat Commun* 4:2575.
- Brahic M, Bousset L, Bieri G, Melki R, Gitler AD (2016) Axonal transport and secretion of fibrillar forms of α -synuclein, A β ₄₂ peptide and HTTExon 1. *Acta Neuropathol* 131:539–548.
- Brundin P, Melki R, Kopito R (2010) Prion-like transmission of protein aggregates in neurodegenerative diseases. *Nat Rev Mol Cell Biol* 11:301–307.
- Cioni JM, Lin JQ, Holtermann AV, Koppers M, Jakobs MAH, Azizi A, Turner-Bridger B, Shigeoka T, Franze K, Harris WA, Holt CE (2019) Late endosomes act as mRNA translation platforms and sustain mitochondria in axons. *Cell* 176:56–72. e15.
- Crocker JC, Grier DG (1996) Methods of digital video microscopy for colloidal studies. *J Colloid Interf Sci* 179:298–310.
- Encalada SE, Goldstein LS (2014) Biophysical challenges to axonal transport: motor-cargo deficiencies and neurodegeneration. *Annu Rev Biophys* 43:141–169.
- Fernandopulle MS, Lippincott-Schwartz J, Ward ME (2021) RNA transport and local translation in neurodevelopmental and neurodegenerative disease. *Nat Neurosci* 24:622–632.
- Ghee M, Melki R, Michot N, Mallet J (2005) PA700, the regulatory complex of the 26S proteasome, interferes with alpha-synuclein assembly. *FEBS J* 272:4023–4033.
- Giandomenico SL, Alvarez-Castelao B, Schuman EM (2022) Proteostatic regulation in neuronal compartments. *Trends Neurosci* 45:41–52.
- Golde TE, Borchelt DR, Giasson BI, Lewis J (2013) Thinking laterally about neurodegenerative proteinopathies. *J Clin Invest* 123:1847–1855.
- Gowrishankar S, Yuan P, Wu Y, Schrag M, Paradise S, Grutzendler J, De Camilli P, Ferguson SM (2015) Massive accumulation of luminal protease-deficient axonal lysosomes at Alzheimer's disease amyloid plaques. *Proc Natl Acad Sci U S A* 112:E3699–E3708.
- Guo W, Stoklund Dittlau K, Van Den Bosch L (2020) Axonal transport defects and neurodegeneration: molecular mechanisms and therapeutic implications. *Semin Cell Dev Biol* 99:133–150.
- Hardy J, Revesz T (2012) The spread of neurodegenerative disease. *N Engl J Med* 366:2126–2128.
- Haziza S, et al. (2017) Fluorescent nanodiamond tracking reveals intraneuronal transport abnormalities induced by brain-disease-related genetic risk factors. *Nat Nanotechnol* 12:322–328.
- Jucker M, Walker LC (2018) Propagation and spread of pathogenic protein assemblies in neurodegenerative diseases. *Nat Neurosci* 21:1341–1349.
- Lee WC, Yoshihara M, Littleton JT (2004) Cytoplasmic aggregates trap polyglutamine-containing proteins and block axonal transport in a *Drosophila* model of Huntington's disease. *Proc Natl Acad Sci U S A* 101:3224–3229.
- Li X, Tsolis KC, Koper MJ, Ronisz A, Ospitalieri S, von Arnim CAF, Vandenberghe R, Tousseyn T, Scheuerle A, Economou A, Carpentier S, Otto M, Thal DR (2021) Sequence of proteome profiles in preclinical and symptomatic Alzheimer's disease. *Alzheimers Dement* 17:946–958.
- Liao YC, et al. (2019) RNA granules hitchhike on lysosomes for long-distance transport, using annexin a11 as a molecular tether. *Cell* 179:147–164. e20.
- Marshall KE, Vadukul DM, Staras K, Serpell LC (2020) Misfolded amyloid- β -42 impairs the endosomal-lysosomal pathway. *Cell Mol Life Sci* 77:5031–5043.
- Millecamps S, Julien JP (2013) Axonal transport deficits and neurodegenerative diseases. *Nat Rev Neurosci* 14:161–176.
- Morfini GA, Burns M, Binder LI, Kanaan NM, LaPointe N, Bosco DA, Brown RH, Brown H, Tiwari A, Hayward L, Edgar J, Nave K-A, Garberrn J, Atagi Y, Song Y, Pigino G, Brady ST (2009) Axonal transport defects in neurodegenerative diseases. *J Neurosci* 29:12776–12786.
- Park JC, Jang SY, Lee D, Lee J, Kang U, Chang H, Kim HJ, Han SH, Seo J, Choi M, Lee DY, Byun MS, Yi D, Cho KH, Mook-Jung I (2021) A logical network-based drug-screening platform for Alzheimer's disease representing pathological features of human brain organoids. *Nat Commun* 12:280.
- Renner M, Lacor PN, Velasco PT, Xu J, Contractor A, Klein WL, Triller A (2010) Deleterious effects of amyloid β oligomers acting as an extracellular scaffold for mGluR5. *Neuron* 66:739–754.
- Saez-Atienzar S, Masliah E (2020) Cellular senescence and Alzheimer disease: the egg and the chicken scenario. *Nat Rev Neurosci* 21:433–444.
- Saudou F, Humbert S (2016) The biology of Huntington. *Neuron* 89:910–926.
- Schindelin J, Arganda-Carreras I, Frise E, Kaynig V, Longair M, Pietzsch T, Preibisch S, Rueden C, Saalfeld S, Schmid B, Tinevez JY, White DJ, Hartenstein V, Eliceiri K, Tomancak P, Cardona A (2012) Fiji: an open-source platform for biological-image analysis. *Nat Methods* 9:676–682.
- Shrivastava AN, Kowalewski JM, Renner M, Bousset L, Koulakoff A, Melki R, Giaume C, Triller A (2013) β -amyloid and ATP-induced diffusional trapping of astrocyte and neuronal metabotropic glutamate type-5 receptors. *Glia* 61:1673–1686.
- Shrivastava AN, Redeker V, Fritz N, Pieri L, Almeida LG, Spolidoro M, Liebmann T, Bousset L, Renner M, Léna C, Aperia A, Melki R, Triller A (2015) α -Synuclein assemblies sequester neuronal α 3-Na⁺/K⁺-ATPase and impair Na⁺ gradient. *EMBO J* 34:2408–2423.
- Shrivastava AN, Aperia A, Melki R, Triller A (2017) Physico-pathologic mechanisms involved in neurodegeneration: misfolded protein-plasma membrane interactions. *Neuron* 95:33–50.
- Soto C, Pritzkow S (2018) Protein misfolding, aggregation, and conformational strains in neurodegenerative diseases. *Nat Neurosci* 21:1332–1340.
- Stokin GB, Lillo C, Falzone TL, Brusch RG, Rockenstein E, Mount SL, Raman R, Davies P, Masliah E, Williams DS, Goldstein LS (2005) Axonopathy and transport deficits early in the pathogenesis of Alzheimer's disease. *Science* 307:1282–1288.
- Vadukul DM, Maina M, Franklin H, Nardecchia A, Serpell LC, Marshall KE (2020) Internalisation and toxicity of amyloid- β 1-42 are influenced by its conformation and assembly state rather than size. *FEBS Lett* 594:3490–3503.
- Volpicelli-Daley LA, Gamble KL, Schultheiss CE, Riddle DM, West AB, Lee VM (2014) Formation of α -synuclein Lewy neurite-like aggregates in axons impedes the transport of distinct endosomes. *Mol Biol Cell* 25:4010–4023.
- Walsh DM, Thulin E, Minogue AM, Gustavsson N, Pang E, Teplow DB, Linse S (2009) A facile method for expression and purification of the Alzheimer's disease-associated amyloid beta-peptide. *FEBS J* 276:1266–1281.
- Winckler B, Faundez V, Maday S, Cai Q, Almeida CG, Zhang H (2018) The endolysosomal system and proteostasis: from development to degeneration. *J Neurosci* 38:9364–9374.